Hyperspectral Anomaly Detection by Fractional Fourier Entropy

Ran Tao, *Senior Member, IEEE*, Xudong Zhao, *Student Member, IEEE*, Wei Li, *Senior Member, IEEE*, Heng-Chao Li, *Senior Member, IEEE*, and Qian Du, *Fellow, IEEE*

***Abstract*—Anomaly detection is an important task in hyperspectral remote sensing. Most widely used detectors, such as Reed–Xiaoli (RX), have been developed only using original spectral signatures, which may lack the capability of signal enhancement and noise suppression. In this article, an effective alternative approach, fractional Fourier entropy (FrFE)-based hyperspectral anomaly detection method, is proposed. First, fractional Fourier transform (FrFT) is employed as preprocessing, which obtains features in an intermediate domain between the original reflectance spectrum and its Fourier transform with complementary strengths by space-frequency representations. It is desirable for noise removal so as to enhance the discrimination between anomalies and background. Furthermore, an FrFE-based step is developed to automatically determine an optimal fractional transform order. With a more flexible constraint, i.e., Shannon entropy uncertainty principle on FrFT, the proposed method can significantly distinguish signal from background and noise. Finally, the proposed FrFE-based anomaly detection method is implemented in the optimal fractional domain. Experimental results obtained on real hyperspectral datasets demonstrate that the proposed method is quite competitive.**

***Index Terms*—Anomaly detection, fractional Fourier entropy (FrFE), fractional Fourier transform (FrFT), hyperspectral imagery (HSI), noise suppression.**

I. Introduction

HYPERSPECTRAL imagery (HSI) comprises hundreds of contiguous spectral bands, which enables to distinguish different objects with subtle spectral difference [9], [16], [21]–[23]. Hyperspectral anomaly detection has drawn increasing attention due to its value in many applications, such as search and rescue operations. It does not require any prior target information, which makes it useful in practical situations [8], [15].

Manuscript received April 7, 2019; revised June 28, 2019; accepted September 5, 2019. Date of publication September 23, 2019; date of current version February 4, 2020. This work was supported by the National Natural Science Foundation of China under Grants 61421001, 61701036, and U1833203. *(Corresponding author: Wei Li.)*

R. Tao, X. Zhao, and W. Li are with the School of Information and Electronics, Beijing Institute of Technology, Beijing 100081, China, and also with the Beijing Key Laboratory of Fractional Signals and Systems, Beijing 100081, China (e-mail: rantao@bit.edu.cn; zhaoxudong@bit.edu.cn; liwei089@ieee.org).

H.-C. Li is with the School of Information Science and Technology, Southwest Jiaotong University, Chengdu 610031, China (e-mail: lihengchao_78@163.com).

Q. Du is with the Department of Electrical and Computer Engineering, Mississippi State University, Starkville, MS 39762 USA (e-mail: du@ece.msstate.edu).

Color versions of one or more of the figures in this article are available online at http://ieeexplore.ieee.org.

Digital Object Identifier 10.1109/JSTARS.2019.2940278

The classic Reed–Xiaoli (RX) [5], [26] was developed using the Mahalanobis distance between the pixel under test and the background. Due to its simplicity and satisfying performance, it has become the benchmark of anomaly detection in HSI. Two typical versions are global and local RX [14], [19], which are different in background estimation. The local RX estimates the background statistics according to predefined local windows, and the global RX uses the entire image for background modeling [36]. Recently, there are some other representative detectors [12], [17], such as detections based on collaborative representation [13], low-rank and sparse representation [28], [30], [37], graph pixel selection [29], [38], etc.

The aforementioned methods are based on original reflectance spectrum. None of them consider a spectral transform, e.g., wavelet and curvelet, which have been investigated for HSI compression or classification [1], [25]. There are several advantages of using these transforms, such as noise suppression and spectral decorrelation. For hyperspectral remote sensing images, the imaging process from satellite or airborne sensors is affected by many factors, such as atmospheric conditions, variations of material surface, etc., which may be nonstationary. Nevertheless, fractional Fourier transform (FrFT) is well known to better handle nonstationary noise than the traditional Fourier transform (FT) [4], [6], which motivates us to employ FrFT for hyperspectral anomaly detection.

Actually, FrFT has been studied for remote sensing image analysis. Discrete FrFT was employed to estimate the chirp parameters in synthetic aperture radar (SAR) image [3]. FrFT-based feature extraction was developed for classification of single-look complex SAR images. In [35], the FrFT was adopted to reduce the impact of migration through resolution cell of ship target in inverse SAR. Furthermore, two-dimensional discrete FrFT was employed for pansharpening of multispectral image [27]. A spectral joint FrFT correlation was presented for hyperspectral target detection, where FrFT was utilized to measure the similarity between pixels under test and a few priori known target pixels [33]. However, when applying FrFT in these tasks, how to decide the fractional transform order keeps a critical problem. Thus, an indirect feature of signals in fractional domain, combining two successful components, i.e., FrFT and Shannon entropy, is introduced to solve this problem, which is defined as fractional Fourier entropy (FrFE) [34].

In this article, a novel FrFE-based hyperspectral anomaly detection (FrFE-RX) is proposed. First of all, FrFT is employed as preprocessing to exploit signal representation in an

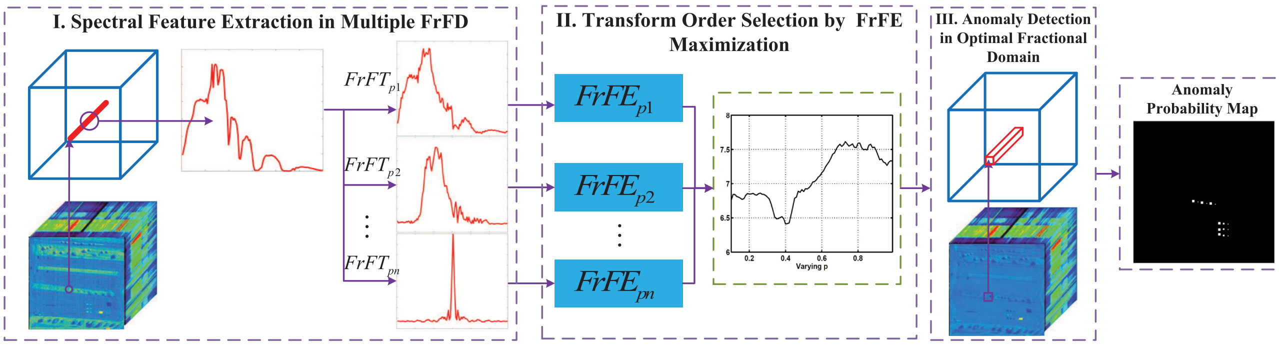

Fig. 1. Flowchart of the proposed FrFE-RX model for hyperspectral anomaly detection. In Part I, red lines indicate the spectral curves of current pixel. Only part of the tested transform orders $p1, p2, \ldots, pn$ are shown for simplification. Then, in Part II, the FrFE values of varying fractional order $p1, p2, \ldots, pn$ are presented for example. In Part III, the pixel in red box is the pixel to be researched.

intermediate domain including both reflectance spectrum and its FT information. Then, an FrFE-based method is developed to automatically determine an optimal fractional transform order using the extracted features, which makes no additional parameter for the proposed framework. Due to the benefits of FrFT, the proposed method can significantly distinguish signal from background and noise. Finally, the RX anomaly detection method is implemented in the optimal fractional domain. Experimental results validated with real hyperspectral datasets demonstrate the effectiveness of the proposed method.

Compared with previous methods, the main contributions of the proposed FrFE-RX are summarized as follows.

1) It is the first time to employ FrFT for exploiting the signal representation in an intermediate domain including both reflectance spectrum and its Fourier domain information, which is beneficial for noise suppression and discrimination enhancement between anomalies and background in HSI.
2) An FrFE-based strategy is developed to automatically determine the parameter of FrFT. With a more flexible constraint, the proposed method can significantly distinguish signal from background and noise. Instead of scanning parameter and adjusting spatial features, the proposed detector directly computes FrFE to select an optimal transform order and discover the internal relationships of hyperspectral pixels in the optimal fractional domain.

The remainder of this article is organized as follows. The proposed framework is introduced in Section II. In Section III, experimental results and analysis are presented. Finally, Section IV summarizes with concluding remarks.

II. Proposed FrFE-Based Hyperspectral Anomaly Detection

The FrFE-RX framework is designed to detect anomaly pixels by distinguishing signal from background in an optimal fractional Fourier domain (FrFD). The framework of the proposed FrFE-RX is illustrated in Fig. 1, which consists of following three parts:

1) multiple domain spectral feature extraction by FrFT (Part I);
2) optimal order selection by FrFE maximization (Part II);
3) RX detector for anomaly detection in the optimal FrFD (Part III).

A. Multiple Domain Spectral Feature Extraction by FrFT

As shown in Part I in Fig. 1, FrFT is first employed as preprocessing to exploit signal representation in an intermediate domain including both reflectance spectrum and its Fourier domain information.

Consider a three-dimensional HSI with resized samples $\mathbf{X} = \{\mathbf{x}_i\}_{i=1}^{N}$ in $\mathbb{R}^d$, where N is the number of pixels and d is the number of spectral bands. In FrFT [4], the original spectrum (space) and frequency characteristics are varied when changing the fractional order. It can be viewed as a transform kernel function with a rotation of the original signal $\mathbf{x}$ from the space-frequency plane to the transform plane. For each pixel $\mathbf{x}$, its representation in FrFT domain is expressed as

$$\mathbf{x}_p(u) = \left(1/d\right)\sum_{s=1}^{d}\mathbf{x}(s)K_p(s,u) \tag{1}$$

with the kernel

$$K_p(s,u) = \begin{cases} A_\phi \exp\left[j\pi\left(s^2\cot\phi - 2su\csc\phi + u^2\cot\phi\right)\right] \\ \phi \neq n\pi \\ \delta\left(s-u\right), \phi = 2n\pi \\ \delta\left(s+u\right), \phi = \left(2n\pm 1\right)\pi \end{cases} \tag{2}$$

where u and s are indices, n is an integer, p is the fractional order of FrFT, and $\phi = p\pi/2$ is the rotation angle. Here, A_ϕ is calculated as

$$A_\phi = \frac{\exp\left[-j\pi\mathrm{sgn}\left(\sin\phi\right)/4 + j\phi/2\right]}{\left|\sin\phi\right|^{1/2}}. \tag{3}$$

When $p = 0$, $\mathbf{x}_p$ is the original spectrum (i.e., $\mathbf{x}$), and when $p = 1$, $\mathbf{x}_p$ is the output of the traditional FT.

When implementing FrFT for each pixel, the essence is to integrate the information of original reflectance spectrum and its frequency domain simultaneously, as shown in Fig. 2. Fig. 2(b) and (c) illustrate the amplitude of FrFT when the fractional order p is 0.7 and 0.9, respectively. It is clearly seen that part of spectral

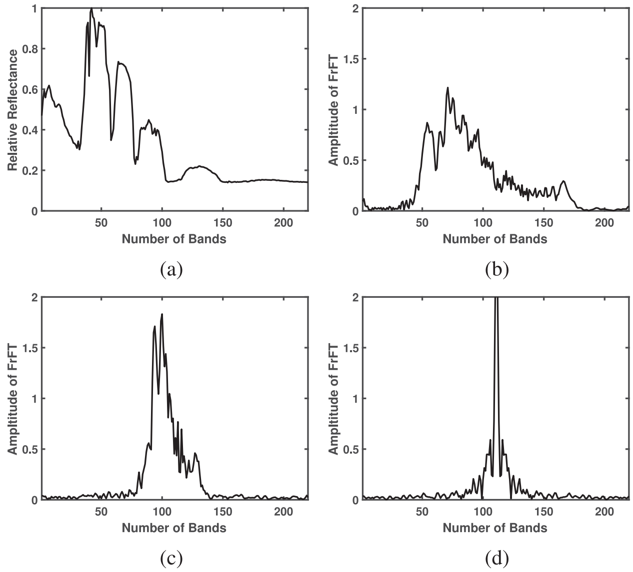

Fig. 2. Illustration with a certain pixel. (a) Original relative reflectance ($p = 0$). (b) Amplitude of FrFT ($p = 0.7$). (c) Amplitude of FrFT ($p = 0.9$). (d) Amplitude of FT ($p = 1$).

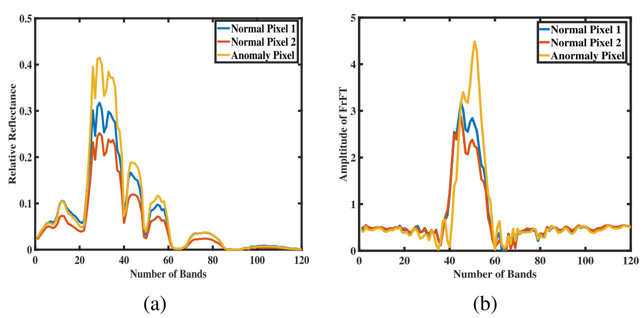

Fig. 3. Illustration with normal and abnormal pixels. (a) Spectral curve of two normal pixels and one anomaly pixel in the original SpecTIR data. (b) Spectral curve of two normal pixels and one anomaly pixel in the FrFT domain when $p = 0.8$.

information is preserved while the energy is concentrated rather than spreading over the entire spectrum. When increasing p, the phenomenon is more obvious. The difference between Fig. 2(c) and (d) is that the latter only contains frequency but not any spectral information.

B. Optimal Order Selection by FrFE Maximization

In Section II-A, the spectral features are extracted in multiple FrFDs. Both the original relative reflectance and amplitude of FrFT information can be used for anomaly detection. Fig. 3 further illustrates spectral discrimination between the original and the FrFT domain using two normal pixels and one anomaly pixel. It is apparent that Fig. 3(b) is much discernible than Fig. 3(a), with higher contrast. Fig. 3 confirms that the discrimination between background and anomalies is more obvious in the new spectral bands. Thus, anomalous pixels are more identifiable.

Furthermore, Fig. 4 illustrates spatial comparison of the 50th spectral band between the original and the FrFT domain using

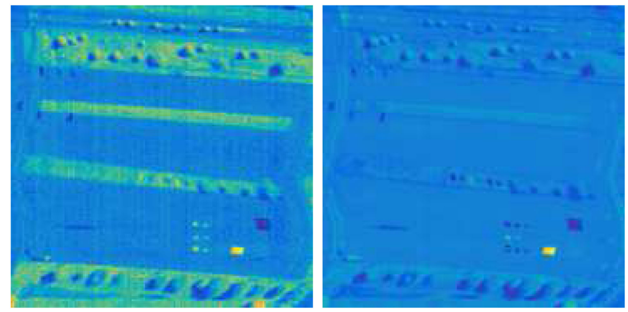

Fig. 4. Illustration with a hyperspectral band. (a) Fiftieth band using the original SpecTIR data. (b) Fiftieth band in the FrFT domain when $p = 0.9$.

an experimental data to be introduced in the next section. Apparently Fig. 4(b) is much clearer than Fig. 4(a), with less noise and higher contrast. Figs. 2–4 confirm that noise suppression can be realized by the FrFT.

In the proposed framework, one of the most important steps is to automatically determine the fractional order (i.e., p) of FrFT. Motivated by aforementioned observations, a simple yet efficient FrFE-based strategy is developed to determine the fractional order p. Entropy measure, which reflects information contained in the produced spectral bands, is widely used for evaluation of image quality [32]. The Shannon entropy is defined as

$$E = -\sum_{i=0}^{L-1} q_i \log(q_i) \tag{4}$$

where L represents gray levels and q_i is the probability of the ith gray level. As the constraint of FT in traditional time–frequency domains, the Shannon entropy uncertainty principle has been discussed [2], [7]. The traditional Shannon entropy uncertainty is defined as

$$E\{|\mathbf{x}(u)|^2\} + E\{|\mathbf{x}(s)|^2\} \geq \ln(\pi e) \tag{5}$$

where $\mathbf{x}(u)$ is the FT of $\mathbf{x}(s)$.

Here, to measure the enhancement of the discrimination between anomalies and background with varying fractional order, FrFE is introduced. Mathematically, Shannon entropy operator E is implemented on the spectrums $\mathbf{X}_p$ obtained by FrFT and the p order FrFE is defined as

$$FrFE_p = E \cdot \mathbf{X}_p. \tag{6}$$

When FrFT was implemented over the hyperspectral images $\mathbf{X}$, the entropy of each band in $\mathbf{X}_p$ is computed and the FrFE of particular bands is obtained with order p.

It is expected that the value of p is optimal if it products the highest quality (i.e., clear with more detailed information) images that further enhance the discrimination between anomalies and background. The optimal p is obtained when E is the maximum. Similar to the traditional Shannon entropy uncertainty principle, the Shannon entropy uncertainty principle in two FrFT domains is the constraint of FrFT [10]:

$$E\{|\mathbf{x}_p(u)|^2\} + E\{|\mathbf{x}(s)|^2\} \geq \ln(\pi e|\sin(p)|) \tag{7}$$

which shows that the Shannon entropy uncertainty principle in two fractional domains is connected with the transform order p. In addition, if $\sin(p) = \pm 1/\pi e$, the bound will be zero, i.e., the bound of Shannon entropy uncertainty principle in two FrFT domains can be zero, which provides the possible better selection in the FrFT domain for enhancing the discrimination between anomalies and background. Compared to Fourier entropy, FrFE order selection is more flexible and possible to maximize.

Then, the optimal fractional transform order can be obtained as

$$lp = \arg\max_p \mathrm{FrFE}_p$$
$$\text{s.t.} E\{|\mathbf{x}_p(u)|^2\} + E\{|\mathbf{x}(s)|^2\} \geq \ln(\pi e|\sin(p)|). \quad (8)$$

When FrFT was implemented over the hyperspectral images, the FrFE can be computed across particular bands. The maximum of FrFE is selected from all bands of the transformed images.

C. Anomaly Detection in Optimal FrFD

With the optimal fractional transform order selected, the traditional RX method can be used to detect anomaly with the maximum discrimination between anomalies and background. Amplitude information (i.e., $\tilde{\mathbf{X}} = |\mathbf{x}_p(u)|$) is used as representative features in the FrFT domain, followed by the classic RX detector [14], [19]. The two competing hypotheses are given by

$$H_0 : \mathbf{X} = \mathbf{n} \quad \text{Anomaly is not present}$$
$$H_1 : \mathbf{X} = a\mathbf{s} + \mathbf{n} \quad \text{Anomaly is present} \quad (9)$$

where $a = 0$ under H_0 and $a > 0$ under H_1, respectively, $\mathbf{n}$ represents the background clutter noise process, and $\mathbf{s}$ is the spectral signature of the signal. The anomaly signature $\mathbf{s}$ and background covariance $\mathbf{C}_b$ are assumed to be unknown. Assume an anomaly pixel $\tilde{\mathbf{X}}$ as the observation test vector, the result of the RX method is described as

$$r(\mathbf{X}) = (\widetilde{\mathbf{X}} - \hat{\mu}_b)^T \hat{\mathbf{C}}_b (\widetilde{\mathbf{X}} - \hat{\mu}_b) \quad (10)$$

where $\hat{\mathbf{C}}_b = \frac{1}{N}\mathbf{X}_b\mathbf{X}_b^T$ is a $d \times d$ covariance matrix of the amplitude of FrFT-transformed $\tilde{\mathbf{X}}$, and mean vector $\boldsymbol{\mu}_b = \sum_{i=1}^{N} \tilde{\mathbf{X}}_i$. The output $r(\mathbf{X})$ is compared with a prescribed threshold η. The pixel is claimed to be an anomaly if $r(\mathbf{X}) > \eta$, otherwise, it is a background pixel. The proposed FrFE-RX anomaly detection algorithm is summarized in Algorithm 1.

III. Experimentation Results and Analysis

In this section, experimental results are presented to illustrate the effectiveness of the FrFE-RX model for hyperspectral images anomaly detection. All the programs are implemented using MATLAB language in a personal computer equipped with Windows 7 and Intel Core i7-6700 CPU @3.40 GHz with 16 GB RAM.

A. Experimental Data

In our experiments, several real hyperspectral images are utilized to demonstrate the effectiveness of the proposed method in anomaly detection.

TABLE I
ABU Dataset With Nine Hyperspectral Images

Images	Captured place	Resolution	Sensor	Fight time
A-1	Los Angeles	7.1 m	AVIRIS	11/9/2011
A-2	Los Angeles	7.1 m	AVIRIS	11/9/2011
A-3	Los Angeles	7.1 m	AVIRIS	11/9/2011
A-4	Gulfport	3.4 m	AVIRIS	7/7/2010
B-1	Cat Island	17.2 m	AVIRIS	9/12/2010
B-2	San Diego	7.5 m	AVIRIS	11/16/2011
U-1	Texas Coast	17.2 m	AVIRIS	8/29/2010
U-2	Texas Coast	17.2 m	AVIRIS	8/29/2010
U-3	Gainesville	3.5 m	AVIRIS	9/4/2010

Algorithm 1: FrFE-RX Model.

Require: original image $\mathbf{X} = \{\mathbf{x}_i\}_{i=1}^N$.
1: **for** all pixels $i = 1, \ldots, n$ **do**
2: Step1: **FrFT for multiple domain feature extraction**
3: For each test pixel $\mathbf{x}_i$, its representation in fractional domains are obtained by 1.
4: Step2: **Order selection by FrFE maximization**
5: For each feature curve extracted in particular p fractional domain, corresponding FrFE is computed by 6.
6: Select the optimal fractional order p to maximize the FrFE by 8.
7: Step3: **Anomaly detection in p fractional domain**
8: For each test pixel $\mathbf{x}_i$, its representation in the optimal p order FrFT domain are obtained by 1.
9: Anomaly probability of the tested pixel is obtained by 10.
10: **end for**
Ensure: anomaly detection map $r(\mathbf{X})$, optimal fractional transform order p.

1) SpecTIR Dataset: The first experimental data were derived from the SpecTIR hyperspectral airborne Rochester experiment [11]. An image area of 180×180 pixels with 120 bands and 1-m spatial resolution is selected for evaluation. Anomalies consist of man-made colorful square fabrics.

2) World Trade Center (WTC) Dataset: The second hyperspectral data were derived from the airborne visible infra-red imaging spectrometer (AVIRIS) over the WTC in New York [24]. An area of 200×200 pixels with 224 bands is selected for the following experiments, where latent fire at the WTC are anomalies. The location information, regarded as anomalies, was provided by the United States Geological Survey.

3) Urban Dataset: The third data were collected by the hyperspectral digital imagery collection experiment (HYDICE) sensor [20]. This urban scene consists of 80×100 pixels. The spatial resolution is approximately 1 m. 175 bands are remained after removal of water vapor absorption bands. There are 21 anomalous pixels, representing cars and roof.

TABLE II
BD, FrFE, AND AUC ANALYSIS WITH VARYING FRACTIONAL ORDER p

	SpecTIR											ABU-A-4										
Order	0	0.1	0.2	0.3	0.4	0.5	0.6	0.7	0.8	0.9	1.0	0	0.1	0.2	0.3	0.4	0.5	0.6	0.7	0.8	0.9	1.0
BD	4.71	4.85	5.69	7.34	11.81	13.65	13.05	19.52	**25.01**	21.50	5.68	8.71	13.00	13.21	12.49	12.81	15.06	15.58	16.52	16.54	**16.97**	11.07
Entropy	5.68	5.69	5.64	5.61	5.63	5.74	5.81	5.92	**6.22**	6.10	6.01	6.31	6.41	6.47	6.39	6.30	6.53	6.59	6.63	6.66	**6.82**	6.76
AUC(%)	99.14	99.16	99.19	99.23	99.45	99.69	99.86	99.88	**99.91**	99.89	99.23	95.25	96.84	97.13	97.29	97.73	97.51	97.55	97.85	98.02	**98.54**	97.19
	WTC											ABU-B-1										
Order	0	0.1	0.2	0.3	0.4	0.5	0.6	0.7	0.8	0.9	1.0	0	0.1	0.2	0.3	0.4	0.5	0.6	0.7	0.8	0.9	1.0
BD	5.95	11.20	13.83	12.57	13.64	14.43	15.42	19.74	23.98	**28.43**	10.39	32.31	31.34	31.69	30.45	26.85	30.36	30.02	36.02	**37.25**	30.48	17.70
Entropy	6.22	6.24	6.22	6.30	6.18	6.36	6.62	6.54	6.68	**7.13**	6.36	4.99	4.98	4.85	4.91	4.84	4.75	4.81	5.47	**5.94**	5.02	4.81
AUC(%)	97.70	98.38	98.47	98.64	98.74	98.69	98.74	98.98	99.33	**99.49**	92.92	98.07	97.27	97.48	97.77	97.62	97.85	98.12	98.25	**98.62**	97.59	92.12
	HYDICE Urban											ABU-U-2										
Order	0	0.1	0.2	0.3	0.4	0.5	0.6	0.7	0.8	0.9	1.0	0	0.1	0.2	0.3	0.4	0.5	0.6	0.7	0.8	0.9	1.0
BD	26.06	28.39	27.06	29.49	28.34	27.72	28.97	**33.42**	28.37	26.91	7.75	11.33	13.78	15.09	15.06	14.85	18.36	**19.34**	16.84	16.78	16.42	9.83
Entropy	7.14	7.25	7.33	7.35	7.42	7.47	7.48	**7.57**	7.55	7.39	6.93	5.59	5.63	5.40	5.53	5.39	5.48	**6.81**	5.95	5.68	5.61	5.21
AUC(%)	98.55	98.61	98.68	98.83	98.78	98.65	99.01	**99.41**	99.33	99.22	97.57	99.36	99.24	99.35	99.29	99.35	99.41	**99.62**	99.50	99.36	99.37	99.08

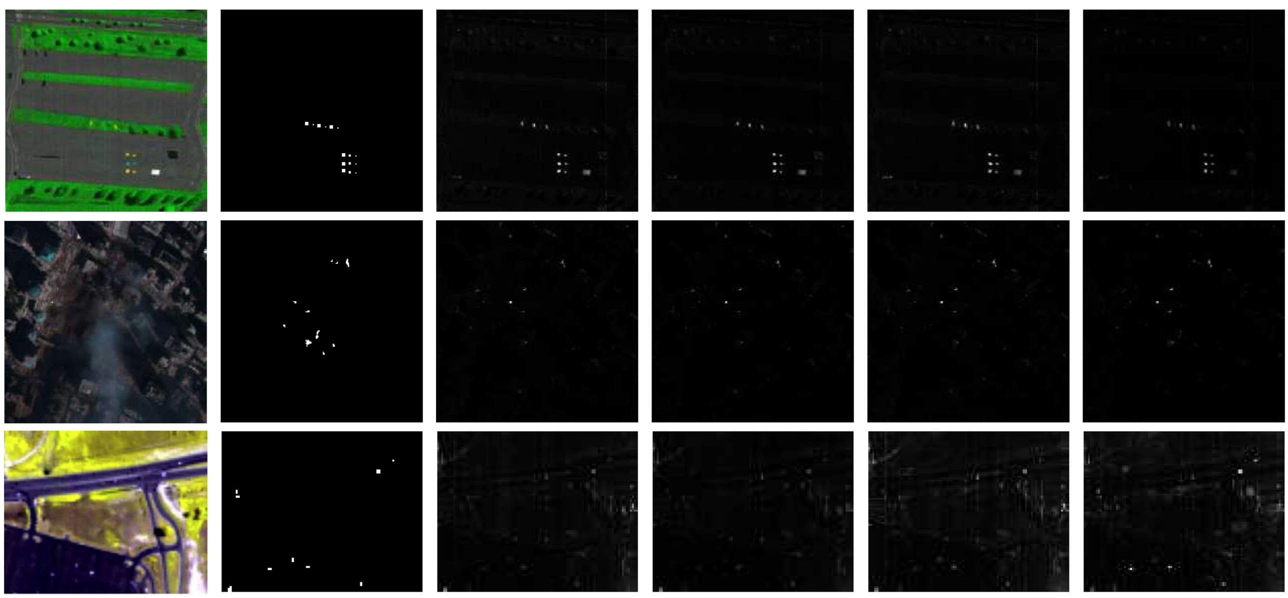

(a) (b) (c) (d) (e) (f)

Fig. 5. Comparison results of the proposed FrFE-RX with other algorithms for anomaly detection using SpecTIR, WTC, and urban datasets. (a) Color composites of input hyperspectral images. (b) Reference detection maps. (c)–(e) Anomaly detection maps of global RX, digital wavelet transform (DWT-RX) [31], and derivatives (Deriv-RX) [18]. (f) Anomaly maps of the proposed FrFE-RX method.

4) Airport-Beach-Urban (ABU) Dataset: The fourth data were sample hyperspectral images in the ABU dataset [12].[1] These images of size 100×100 are extracted from the AVIRIS website.[2] Details of these images are listed in Table I.

B. Analysis on Features in FrFDs

In order to validate the proposed FrFE-RX, this section first analyzes the influence of different fractional orders on the FrFE and the performance of the proposed FrFE-RX method.

One of the most widely used metrics for anomaly detection evaluation is the receiver operating characteristic (ROC) area under the curve (AUC) metric. Table II illustrates AUC (%) and entropy values of varying fractional order p from 0.1 to 0.99 with an interval of 0.01. Means of different intervals (length 0.1) are listed for comparison. Generally, it is found that when changing p, a higher entropy always corresponds to a larger AUC value. Take the SpecTIR data for example, when the range of fractional order p is between 0.7 to 0.9, the AUC value can reach 99.9% or even larger. This is due to the fact that a higher entropy means better image quality, which increases the separability of anomalies and background.

Bhattacharyya distance (BD) is then employed to measure the separability of classes, where a larger value indicates better discrimination. Table II lists the results when p is changed from 0 to 1. Obviously, when $p = 0.8$, the highest BD value is obtained. Note that for the three experimental data, almost all the BD values are larger than those when $p = 0$ or $p = 1$, which further confirms that features in the FrFT domain are more discriminative in separation of anomalies and background.

[1] http://xudongkang.weebly.com/
[2] http://aviris.jpl.nasa.gov/

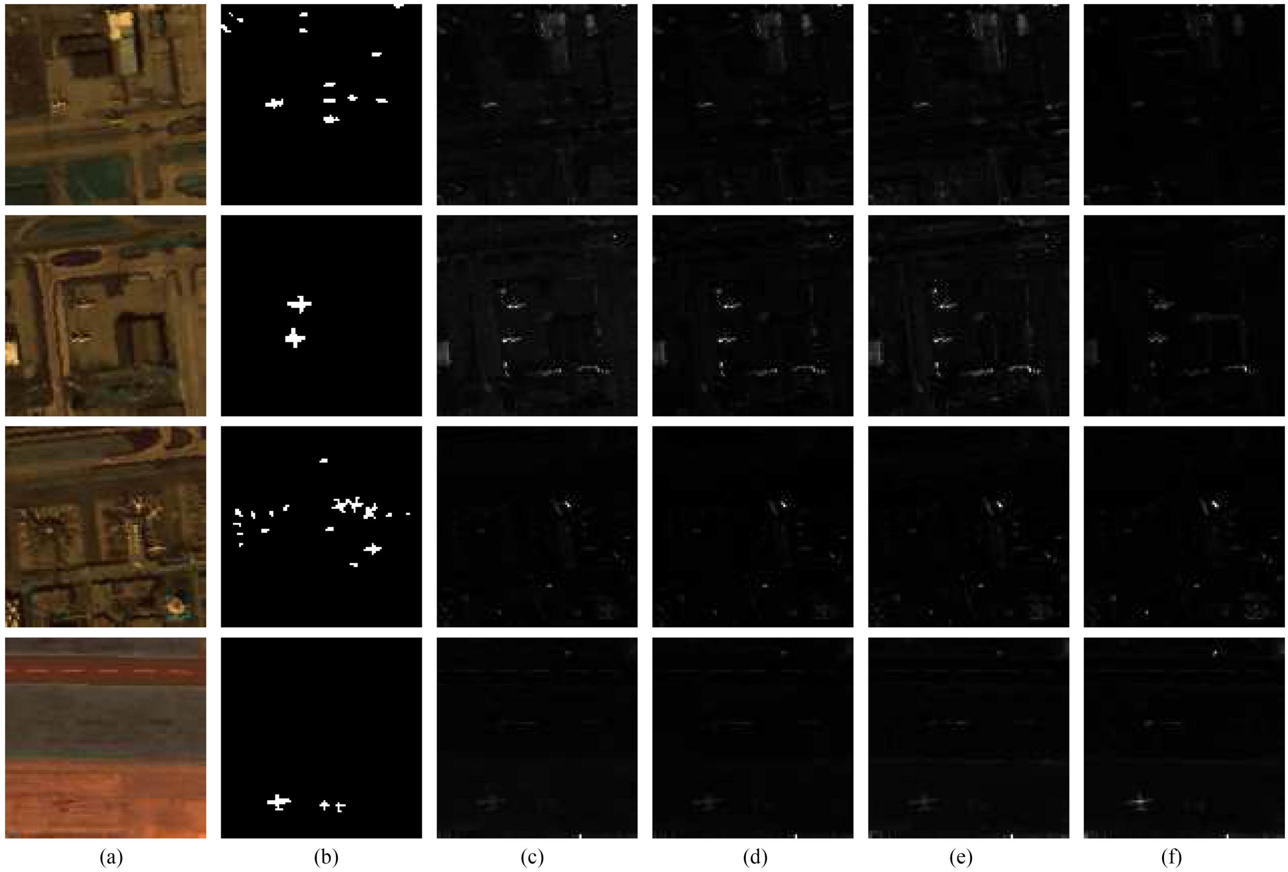

Fig. 6. Comparison results of the proposed FrFE-RX with other algorithms for anomaly detection using ABU-A datasets. (a) Color composites of input hyperspectral images. (b) Reference detection maps. (c)–(e) Anomaly detection maps of global RX, digital wavelet transform (DWT-RX) [31], and derivatives (Deriv-RX) [18]. (f) Anomaly maps of the proposed FrFE-RX method.

With all the aforementioned quantitative BD, FrFE, and AUC comparison under varying fractional order p, we can see obviously in Table II that an optimal fractional order of the example datasets leads to a larger BD, and the FrFT can produce a better AUC. When the range of fractional order is between 0.6–0.9, the BD values increase as well as the FrFE, which means corresponding growth of the discrimination between anomalies band background. Furthermore, the enhancement of discrimination leads to better detection performance measured by AUC.

C. Detection Performance

In this section, the anomaly detection performance of the proposed FrFE-RX is evaluated. In our strategy, FrFT is mainly employed to exploit features from reflectance spectrum, followed by the Global-RX. Other feature extraction methods, such as discrete wavelet transform (DWT) [31] and spectral derivatives [18], are used for comparison, which are denoted as DWT-RX and Deriv-RX, respectively. All the detectors are implemented with optimal parameters. For DWT-RX, Haar wavelet and one-level decomposition are carried out according to our empirical study. For Deriv-RX, stable detection performance is obtained when the derivative step is set to 4.

TABLE III
AUC VALUES (%) OF THE PROPOSED METHOD AND BASELINES

	Global-RX	DFT-RX	DWT-RX	Deriv-RX	FrFE-RX
SpecTIR	99.14	99.23	99.68	99.80	**99.91**
WTC	97.70	92.92	98.02	98.82	**99.49**
Urban	98.55	97.57	98.98	98.73	**99.41**
ABU-Airport Scenes					
ABU-A1	82.21	83.29	86.45	84.56	**90.81**
ABU-A2	84.04	88.14	90.77	88.39	**96.90**
ABU-A3	92.88	86.23	98.73	91.57	**94.24**
ABU-A4	95.26	97.19	97.57	96.72	**98.54**
ABU-Beach Scenes					
ABU-B1	98.07	92.12	97.52	98.18	**98.62**
ABU-B2	**99.99**	99.84	99.98	**99.99**	99.97
ABU-Urban Scenes					
ABU-U1	99.07	79.56	99.10	99.18	**99.18**
ABU-U2	99.46	99.08	99.45	99.48	**99.62**
ABU-U3	95.13	94.06	96.34	95.01	**96.84**

Experiments are performed on the 12 datasets, and the optimal results of RX, Deriv-RX, DWT-RX, and FrFE-RX are reported in Figs. 5–7 according to the corresponding AUC performances. For each method, the AUC scores are presented in Table III. DFT-RX (i.e., $p = 1$) is also included, which fails for detection task, especially for the WTC data. There is no doubt that the proposed FrFE-RX has the largest value. The best scores are

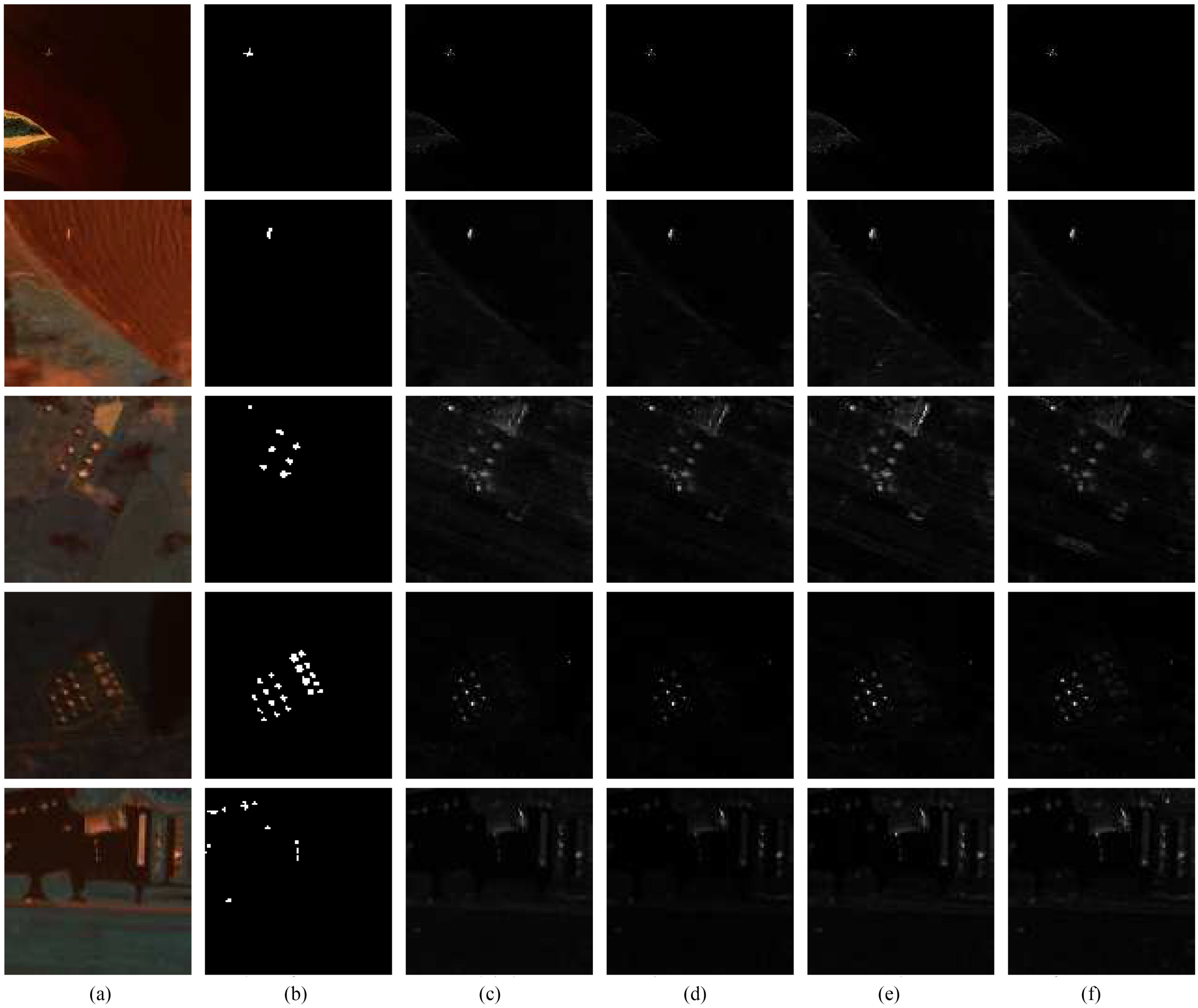

Fig. 7. Comparison results of the proposed FrFE-RX with other algorithms for anomaly detection using ABU-B and ABU-U datasets. (a) Color composites of input hyperspectral images. (b) Reference detection maps. (c)–(e) Anomaly detection maps of global RX, digital wavelet transform (DWT-RX) [31], and derivatives (Deriv-RX) [18]. (f) Anomaly maps of the proposed FrFE-RX method.

highlighted in bold for each images. As shown in Table III, the proposed FrFE-RX method achieves the best scores on most of the hyperspectral images.

By examining the detection maps visually, we find that the FrFE-RX tends to be more sensitive to the anomaly objects of different sizes, even though it does not involve multiscale processing as the DWT. For example, in Fig. 5(c), the anomaly objects in the sea can be well detected by the DWT-RX and FrFE-RX. However, the DWT-RX needs multiscale processing that blurs image edges and, thus, decreasing its detection accuracy. When compared with other anomaly detection methods, the major advantage of the proposed FrFE-RX is its discrimination between anomalies and background. The energy concentration of FrFT in the optimal FrFD greatly helps in detecting anomalies. In general, the detection maps are consistent with the AUC values listed in Table III, which indicates the competitive performance of the proposed FrFE-RX method for hyperspectral anomaly detection.

Fig. 8 illustrates ROC curves for the proposed FrFE-RX and other comparison methods. It is obvious that the proposed method always offers the best detection performance even when the probability of false alarm (P_f) is extremely low. Take the SpecTIR data for example, as shown in Fig. 9, when P_f is 0.01, the probability of detection (P_d) is 100%, whereas others are less than 95%. As shown in Fig. 8(c), when P_d is 95%, the probability of false alarm (P_f) is 0.02%, whereas others are higher than 0.05%.

Table IV further lists the statistical significance of performance difference between the proposed FrFE-RX and the other three detectors. For each comparison, standard error of an AUC is first calculated according to the Wilcoxon statistic, and the Z value of a pair of methods is then calculated based on the difference between the AUC and the standard error. Note that Z value larger than 2.58 means that two ROC curves are statistically different at the 99% confidence level, and when the calculated significance level (i.e., p value) is less than 0.05, the two results

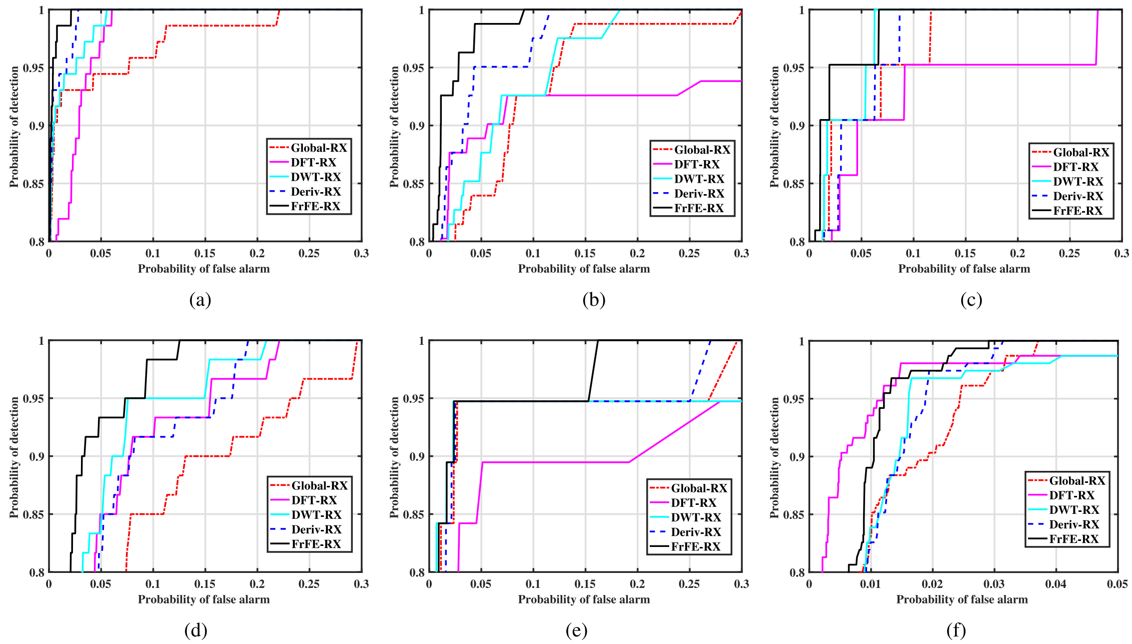

Fig. 8. ROC curves of anomaly detectors using experimental datasets. Detection performances of Global-RX, DFT-RX, DWT-RX, Deriv-RX, and proposed FrFE-RX are depicted. (a) SpecTIR. (b) WTC. (c) Urban. (d) ABU-A-4. (e) ABU-B-1. (f) ABU-U-2.

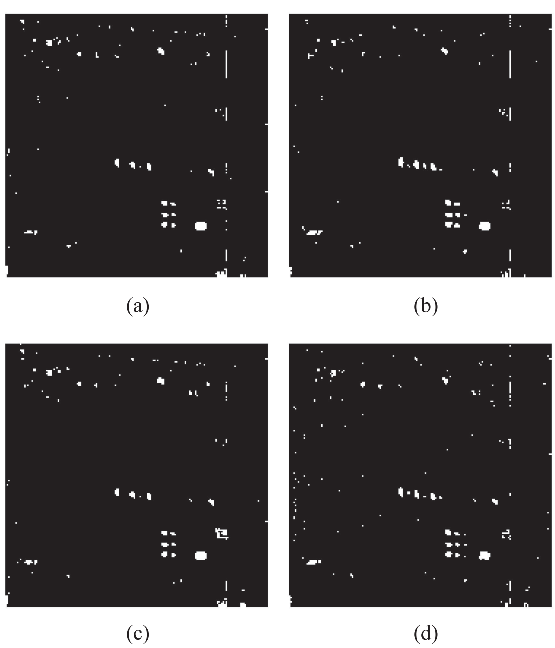

Fig. 9. Detection maps using the SpecTIR data when $P_f = 0.01$. (a) Global-RX: $P_d = 91:67\%$. (b) DWT-RX: $P_d = 94:44\%$. (c) Deriv-RX: $P_d = 91:67\%$. (d) FrFT-RX: $P_d = 100\%$.

are statistically different. Thus, for most situations, the proposed FrFE-RX offers statistically significant improvement with the 99% confidence.

The computational complexity of the aforementioned anomaly detection methods is summarized in Table V. All the average run time in Table V are measured in seconds with

TABLE IV
STATISTICAL SIGNIFICANCE OF THE DIFFERENCE BETWEEN THE PROPOSED METHOD WITH OTHER DETECTORS

FrFT-RX vs.	AUC(%) difference	Standard error	Z Statistic	P value	Significant ? (99% confidence)
			SpecTIR		
Global-RX	0.78	0.00111	7.028	< 0.0001	Yes
DWT-RX	0.24	0.00046	5.193	< 0.0001	Yes
Deriv-RX	0.12	0.00032	3.684	0.0002	Yes
			WTC		
Global-RX	1.76	0.00257	6.846	< 0.0001	Yes
DWT-RX	1.44	0.00228	6.315	< 0.0001	Yes
Deriv-RX	0.64	0.00143	4.470	< 0.0001	Yes
			HYDICE Urban		
Global-RX	0.73	0.00184	3.704	0.0002	Yes
DWT-RX	0.30	0.00150	1.667	0.0956	No
Deriv-RX	0.55	0.00166	3.004	0.0027	Yes
			ABU-A-4		
Global-RX	1.20	0.00314	3.809	< 0.0001	Yes
DWT-RX	0.17	0.00086	1.946	0.0516	No
Deriv-RX	0.55	0.00131	4.170	< 0.0001	Yes
			ABU-B-1		
Global-RX	0.53	0.00639	0.833	0.4046	No
DWT-RX	0.15	0.00179	0.824	0.4101	No
Deriv-RX	0.59	0.00691	0.860	0.3898	No
			ABU-U-2		
Global-RX	0.59	0.00277	2.109	0.0349	No
DWT-RX	0.64	0.00215	2.967	0.0030	Yes
Deriv-RX	0.70	0.00408	1.706	0.0879	No

TABLE V
EXECUTION TIME (IN SECONDS) IN THE FOUR EXPERIMENTAL DATASETS

Images (size)	Methods			
	Global-RX	DWT-RX	Deriv-RX	FrFE-RX
SpecTIR (180×180)	0.23	34.19	0.26	2.10
WTC (200×200)	0.34	58.32	0.39	2.81
Urban (80×100)	0.07	4.27	0.08	0.69
Average ABU (100×100)	0.10	5.82	0.10	0.81

MATLAB implementation. As shown in Table V, the proposed anomaly detection method is very fast, taking about 0.69 s for the urban dataset. This is due to the selection of optimal fractional order that can be computed by FrFE maximization. Thus, the real application of the proposed FrFE-RX will be a relatively easy task.

IV. Conclusion

In this article, an interesting FrFE-based hyperspectral anomaly detection was proposed. First, FrFT was implemented to exploit effective representation in an intermediate domain including both the original reflectance spectrum and its FT information. Furthermore, the proposed FrFE-based method can automatically estimate an optimal fractional order, which resulted in no additional parameter in the proposed framework to be tuned. Experiments with 12 real hyperspectral data demonstrated that by using the FrFT, discrimination between anomalies and background is enhanced. When compared with other transforms for anomaly detection, the proposed method can outperform.

References

[1] N. Amrani, J. Serra-Sagrista, V. Laparra, M. W. Marcellin, and J. Malo, "Regression wavelet analysis for lossless coding of remote-sensing data," *IEEE Trans. Geosci. Remote Sens.*, vol. 54, no. 9, pp. 5616–5627, Sep. 2016.

[2] I. Bialynicki-Birula, "Entropic uncertainty relations in quantum mechanics," in *Quantum Probability and Applications II*. Berlin, Germany: Springer, 1985, pp. 90–103.

[3] J. B. Campbell *et al.*, "Remote vibration estimation using displace-phase-center antenna SAR for strong clutter environments," *IEEE Trans. Geosci. Remote Sens.*, vol. 56, no. 5, pp. 2735–2747, May 2018.

[4] C. Candan, M. A. Kutay, and H. Ozaktas, "The discrete fractional Fourier transform," *IEEE Trans. Signal Process.*, vol. 48, no. 5, pp. 1329–1337, May 2000.

[5] C. I. Chang and S. S. Chiang, "Anomaly detection and classification for hyperspectral imagery," *IEEE Trans. Geosci. Remote Sens.*, vol. 40, no. 6, pp. 1314–1325, Jun. 2002.

[6] S. Chen, S. Zhang, H. Zhao, and Y. Chen, "A new chirp scaling algorithm for highly squinted missile-borne SAR based on FrFT," *IEEE J. Sel. Topics Appl. Earth Observ. Remote Sens.*, vol. 8, no. 8, pp. 3977–3987, Aug. 2015.

[7] A. Dembo, T. M. Cover, and J. A. Thomas, "Information theoretic inequalities," *IEEE Trans. Inf. Theory*, vol. 37, no. 6, pp. 1501–1518, Nov. 1991.

[8] B. Du and L. Zhang, "A discriminative metric learning based anomaly detection method," *IEEE Trans. Geosci. Remote Sens.*, vol. 52, no. 11, pp. 6844–6857, Nov. 2014.

[9] M. Fauvel, Y. Tarabalka, J. A. Benediktsson, J. Chanussot, and J. C. Tilton, "Advances in spectral-spatial classification of hyperspectral images," *Proc. IEEE*, vol. 101, no. 3, pp. 652–675, Mar. 2013.

[10] X. Guanlei, W. Xiaotong, and X. Xiaogang, "Generalized entropic uncertainty principle on fractional Fourier transform," *Signal Process.*, vol. 89, no. 12, pp. 2692–2697, 2009.

[11] J. A. Herweg *et al.*, "SpecTIR hyperspectral airborne Rochester experiment data collection campaign," *SPIE Defense, Secur., Sens.*, vol. 8390, 2012, Art. no. 839028.

[12] X. Kang, X. Zhang, S. Li, K. Li, J. Li, and J. A. Benediktsson, "Hyperspectral anomaly detection with attribute and edge-preserving filters," *IEEE Trans. Geosci. Remote Sens.*, vol. 55, no. 10, pp. 5600–5611, Oct. 2017.

[13] W. Li and Q. Du, "Collaborative representation for hyperspectral anomaly detection," *IEEE Trans. Geosci. Remote Sens.*, vol. 53, no. 3, pp. 1463–1474, Mar. 2015.

[14] W. Li and Q. Du, "Decision fusion for dual-window-based hyperspectral anomaly detector," *J. Appl. Remote Sens.*, vol. 9, no. 1, 2015, Art. no. 097297.

[15] W. Li and Q. Du, "A survey on representation-based classification and detection in hyperspectral remote sensing imagery," *Pattern Recognit. Lett.*, vol. 83, pp. 115–123, 2016.

[16] W. Li, Q. Du, and B. Zhang, "Combined sparse and collaborative representation for hyperspectral target detection," *Pattern Recognit.*, vol. 48, no. 12, pp. 3904–3916, 2015.

[17] W. Li, G. Wu, and Q. Du, "Transferred deep learning for anomaly detection in hyperspectral imagery," *IEEE Geosci. Remote Sens. Lett.*, vol. 14, no. 5, pp. 597–601, May 2017.

[18] D. Liu L. Han, "Spectral curve shape matching using derivatives in hyperspectral images," *IEEE Geosci. Remote Sens. Lett.*, vol. 14, no. 4, pp. 504–508, Apr. 2017.

[19] W. M. Liu and C. I. Chang, "Multiple-window anomaly detection for hyperspectral imagery," *IEEE J. Sel. Topics Appl. Earth Observ. Remote Sens.*, vol. 6, no. 2, pp. 644–658, Apr. 2013.

[20] L. Ma, M. M. Crawford, and J. Tian, "Local manifold learning based k-nearest-neighbor for hyperspectral image classification," *IEEE Trans. Geosci. Remote Sens.*, vol. 48, no. 11, pp. 4099–4109, Nov. 2010.

[21] S. Mei, J. Ji, Y. Geng, Z. Zhang, X. Li, and Q. Du, "Unsupervised spatial-spectral feature learning by 3D convolutional autoencoder for hyperspectral classification," *IEEE Trans. Geosci. Remote Sens.*, vol. 57, no. 9, pp. 6808–6820, Sep. 2019.

[22] S. Mei *et al.*, "Learning sensor-specific spatial-spectral features of hyperspectral images via convolutional neural networks," *IEEE Trans. Geosci. Remote Sens.*, vol. 55, no. 8, pp. 4520–4533, Aug. 2017.

[23] S. Mei, Y. Xin, J. Ji, Y. Zhang, W. Shuai, and D. Qian, "Hyperspectral image spatial super-resolution via 3D full convolutional neural network," *Remote Sens.*, vol. 9, no. 11, 2017, Art. no. 1139.

[24] J. M. Molero, E. M. Garzon, I. Garcia, and A. Plaza, "Analysis and optimizations of global and local versions of the RX algorithms for anomaly detection in hyperspectral data," *IEEE J. Sel. Topics Appl. Earth Observ. Remote Sens.*, vol. 6, no. 2, pp. 801–814, Apr. 2013.

[25] T. Qiao *et al.*, "Effective denoising and classification of hyperspectral image using curvelet transform and singular spectrum analysis," *IEEE Trans. Geosci. Remote Sens.*, vol. 55, no. 1, pp. 119–133, Jan. 2017.

[26] I. S. Reed and X. Yu, "Adaptive multiple-band CFAR detection of an optical pattern with unknown spectral distribution," *IEEE Trans. Acoust., Speech, Signal Process.*, vol. 38, no. 10, pp. 1760–1770, Oct. 1990.

[27] N. Saxena and K. K. Sharma, "Pansharpening scheme using filtering in two-dimensional discrete fractional Fourier transform," *IET Image Process.*, vol. 12, no. 6, pp. 1013–1019, 2018.

[28] W. Sun, T. Long, X. Yan, D. Bo, and D. Qian, "A randomized subspace learning based anomaly detector for hyperspectral imagery," *Remote Sens.*, vol. 10, no. 3, 2018, Art. no. 417.

[29] W. Sun and D. Qian, "Graph-regularized fast and robust principal component analysis for hyperspectral band selection," *IEEE Trans. Geosci. Remote Sens.*, vol. 56, no. 6, pp. 3185–3195, Jun. 2018.

[30] W. Sun, G. Yang, J. Li, and D. Zhang, "Randomized subspace-based robust principal component analysis for hyperspectral anomaly detection," *J. Appl. Remote Sens.*, vol. 12, no. 1, pp. 1–19, 2018.

[31] Y. Tang, Y. Lu, and H. Yuan, "Hyperspectral image classification based on three-dimensional scattering wavelet transform," *IEEE Trans. Geosci. Remote Sens.*, vol. 53, no. 5, pp. 2467–2480, May 2015.

[32] D. Tsai, Y. Lee, and E. Matsuyama, "Information entropy measure for evaluation of image quality," *J. Digit. Imag.*, vol. 21, no. 3, pp. 338–347, 2008.

[33] Q. Wang, Q. Guo, J. Zhou, and Q. Lin, "Nonlinear joint fractional Fourier transform correlation for target detection in hyperspectral image," *Opt. Laser Technol.*, vol. 44, pp. 1897–1904, 2012.

[34] S. Wang *et al.*, "Pathological brain detection by a novel image feature—Fractional Fourier entropy," *Entropy*, vol. 17, no. 12, pp. 8278–8296, 2015.

[35] Y. Wang and X. Chen, "3-D interferometric inverse synthetic aperture radar imaging of ship target with complex motion," *IEEE Trans. Geosci. Remote Sens.*, vol. 56, no. 7, pp. 3693–3708, Jul. 2018.

[36] Z. Wu, W. Zhu, J. Chanussot, Y. Xu, and S. Osher, "Hyperspectral anomaly detection via global and local joint modeling of background," *IEEE Trans. Signal Process.*, vol. 67, no. 14, pp. 3858–3869, Jul. 2019.

[37] Y. Xu, Z. Wu, J. Li, A. Plaza, and Z. Wei, "Anomaly detection in hyperspectral images based on low-rank and sparse representation," *IEEE Trans. Geosci. Remote Sens.*, vol. 54, no. 4, pp. 1990–2000, Apr. 2016.

[38] Y. Yuan, D. Ma, and Q. Wang, "Hyperspectral anomaly detection by graph pixel selection," *IEEE Trans. Cybern.*, vol. 46, no. 12, pp. 3123–3134, Dec. 2016.

Ran Tao (M'00–SM'04) received the B.S. degree from the Electronic Engineering Institute of PLA, Hefei, China, in 1985, and the M.S. and Ph.D. degrees from the Harbin Institute of Technology, Harbin, China, in 1990 and 1993, respectively.

He was a Senior Visiting Scholar with the University of Michigan, Ann Arbor, MI, USA, and the University of Delaware, Newark, DE, USA, in 2001 and 2016, respectively. He is currently a Professor with the School of Information and Electronics, Beijing Institute of Technology, Beijing, China. He has been a Chief Professor of the Creative Research Groups, National Natural Science Foundation of China since 2014, and he was a Chief Professor of the Program for Changjiang Scholars and Innovative Research Team in University during 2010–2012. He has authored/coauthored three books and more than 100 peer-reviewed journal articles. His current research interests include fractional Fourier transform and its applications, theory, and technology for radar and communication systems.

Prof. Tao is a fellow of the Institute of Engineering and Technology and the Chinese Institute of Electronics. He was a recipient of the National Science Foundation of China for Distinguished Young Scholars in 2006, and a Distinguished Professor of Changjiang Scholars Program in 2009. He is currently the Vice-Chair of the IEEE China Council. He is also the Vice-Chair of the International Union of Radio Science (URSI) China Council and a member of Wireless Communication and Signal Processing Commission, URSI. He was a recipient of the First Prize of Science and Technology Progress in 2006 and 2007, and the First Prize of Natural Science in 2013, both awarded by the Ministry of Education.

Xudong Zhao (S'19) received the B.S. degree in science and technology in 2016 from the Department of Electronic Information, Beijing Institute of Technology, Beijing, China, where he is currently working toward the Ph.D. degree in information and communication engineering under the supervision of Dr. R. Tao.

His research interests include fractional Fourier transform, graph theory, and remote sensing image process.

Wei Li (S'11–M'13–SM'16) received the B.E. degree in telecommunications engineering from Xidian University, Xi'an, China, in 2007, the M.S. degree in information science and technology from Sun Yat-Sen University, Guangzhou, China, in 2009, and the Ph.D. degree in electrical and computer engineering from Mississippi State University, Starkville, MS, USA, in 2012.

Subsequently, he spent one year as a Postdoctoral Researcher with the University of California, Davis, CA, USA. He is currently a Professor with the School of Information and Electronics, Beijing Institute of Technology, Beijing, China. His research interests include hyperspectral image analysis, pattern recognition, and data compression.

Dr. Li is an active reviewer for the IEEE Transactions on Geoscience and Remote Sensing, the IEEE Geoscience Remote Sensing Letters, and the IEEE Journal of Selected Topics in Applied Earth Observations and Remote Sensing (JSTARS). He is currently serving as an Associate Editor for the IEEE Signal Processing Letters. He has served as a Guest Editor for special issues of the *Journal of Real-Time Image Processing, Remote Sensing*, and IEEE JSTARS. He was the recipient of the 2015 Best Reviewer Award from the IEEE Geoscience and Remote Sensing Society for his service for IEEE JSTARS.

Heng-Chao Li (S'06–M'08–SM'14) received the B.Sc. and M.Sc. degrees from Southwest Jiaotong University, Chengdu, China, in 2001 and 2004, respectively, and the Ph.D. degree from the Graduate University of Chinese Academy of Sciences, Beijing, China, in 2008, all in information and communication engineering.

From 2013 to 2014, he was a Visiting Scholar with the University of Colorado, Boulder, CO, USA. He is currently a Professor with the Sichuan Provincial Key Laboratory of Information Coding and Transmission, Southwest Jiaotong University. His research interests include the statistical analysis of synthetic aperture radar images, remote sensing image processing, and signal processing in communications.

Dr. Li was a recipient of several scholarships or awards, especially including the Special Grade of the financial support from the China Postdoctoral Science Foundation in 2009 and the New Century Excellent Talents in University from the Ministry of Education of China in 2011. He serves as an Associate Editor for the IEEE Journal of Selected Topics in Applied Earth Observations and Remote Sensing (JSTARS). He has been a reviewer for several international journals and conferences, such as IEEE Transactions on Geoscience and Remote Sensing, IEEE JSTARS, IEEE Geoscience and Remote Sensing Letters, IEEE Transactions on Image Processing, *IET Radar, Sonar and Navigation*, *IET Signal Processing*, *IET Image Processing*, *Pattern Recognition*, *International Journal of Remote Sensing*, *Remote Sensing*, and *Canadian Journal of Remote Sensing*.

Qian Du (S'98–M'00–SM'05–F'18) received the Ph.D. degree in electrical engineering from the University of Maryland at Baltimore, Baltimore, MD, USA, in 2000.

She is currently the Bobby Shackouls Professor with the Department of Electrical and Computer Engineering, Mississippi State University, Starkville, MS, USA, and also an Adjunct Professor with the College of Surveying and Geo-Informatics, Tongji University, Shanghai, China. Her research interests include hyperspectral remote sensing image analysis and applications, pattern classification, data compression, and neural networks.

Dr. Du is a fellow of the SPIC International Society for Optics and Photonics. She was the Chair of the Remote Sensing and Mapping Technical Committee, International Association for Pattern Recognition, from 2010 to 2014. She was a recipient of the 2010 Best Reviewer Award from the IEEE Geoscience and Remote Sensing Society (GRSS). She served as a Co-Chair of the Data Fusion Technical Committee of IEEE GRSS from 2009 to 2013. She was the General Chair for the fourth IEEE GRSS Workshop on Hyperspectral Image and Signal Processing: Evolution in Remote Sensing, held at Shanghai, China, in 2012. She served as an Associate Editor for the IEEE Journal of Selected Topics in Applied Earth Observations and Remote Sensing (JSTARS), *Journal of Applied Remote Sensing*, and IEEE Signal Processing Letters. Since 2016, she has been the Editor-in-Chief for IEEE JSTARS.